Geographic-Information-based Stochastic Optimization Model for Multi-Microgrid Planning

Enrique Gabriel Vera[a], Claudio Cañizares[a], Mehrdad Pirnia[a]

[a] *University of Waterloo, Waterloo, Ontario, Canada*

Abstract

This paper presents a model for the realistic planning of multi-microgrids in the context of Active Distribution Networks with the assistance of Geographic Information Systems. The model considers the distribution system grid as well as the geographic features of the Region of Interest. It also includes long-term purchase decisions and short-term operational constraints, and considers uncertainties associated with electricity demand and Renewable Energy Resources using an existing Two-Stage Stochastic Programming approach. Geographic Information Systems along with Deep Learning are used to estimate the areas of rooftops within the Region of Interest and model the Low Voltage grid. The planning model is used to study the feasibility of implementing a multi-microgrid system consisting of 4 individual microgrids at an Active Distribution Network in a municipality in the state of São Paulo, Brazil. The results of the model presented in this paper are compared with the results obtained using Monte Carlo Simulations and an existing, less detailed, Two Stage Stochastic model. It is demonstrated that the stochastic solutions are close to those obtained with Monte Carlo at a lower computational cost, and that the use of Geographic Information allows to determine both the capacity and location of the PV panels, batteries, and distribution transformers on the microgrids grid, thus providing more precise and useful planning results.

Keywords:
Active distribution systems, deep learning, energy planning, geographic information systems, multi-microgrids, renewable energy sources, stochastic optimization, uncertainties.

1. Introduction

Global warming is a serious issue that is being tackled from various fronts, one of them being the decarbonization of electrical energy systems, which may be addressed by introducing clean Distributed Energy Resources (DERs) such as Renewable Energy Sources (RESs) and Energy Storage Systems (ESSs) [1]. These types of technologies can be clustered to form Microgrids (MGs), which have the potential to provide access to cheaper, cleaner, and more flexible and reliable electricity [2, 3, 4, 5]. In addition, independent MGs can be interconnected to form Multi-Microgrid (MMG) systems in the context of Active Distribution Networks (ADNs), bringing valuable benefits such as energy use optimization, power quality and stability improvements, network congestion reductions, transmission and distribution system investment deferrals, efficiency, reliability, and flexibility enhancements for both costumers and utilities [6, 7, 8, 9].

MMG systems can be effectively integrated within ADNs. Thus, to analyze integration barriers and future real-time operation challenges of MMGs, the development of a proper long-term planning framework that considers realistic parameters and conditions associated with the location of RES is necessary. The planning of MMG systems is a decision-making issue, where technical and economic criteria must be considered to select the optimal location and mix of generation and storage resources that are necessary to satisfy the end-users energy requirements. Therefore, optimization models that include a wide variety of constraints are used, in which the complexity of the solution depends on the selected approach and degree of detail considered for modeling. In addition, planning models are prone to uncertainties associated with demand and availability of resources, which need to be included in the mathematical formulation to obtain results that are more accurate.

Geographical Information Systems (GIS) are being applied to power systems, improving the management and development of conventional generation sources, addressing location-related problems, and helping in ADN real-time operation and maintenance when integrated with Supervisory Control and Data Acquisition (SCADA) systems [10]. Therefore, GIS allow the inclusion of georeferenced parameters within the optimization formulation, thus allowing the visualization of the results over the real network using maps. This can help enhance the decision-making process while offering tools to better understand and interpret the results, which facilitates its implementation.

The identification and estimation of renewable resources using GIS have been studied by different authors. For instance, in [11], wind energy potential with consideration of environmental impacts is studied in different Turkey provinces to identify sites for wind turbine installation. Similarly, in [12], an approach is proposed to identify suitable locations in the Canary Islands for the installation of wind turbines, considering technical, economic, and spatial constraints. GIS-based imagery analysis can

Glossary

ADN	Active Distribution Network	ML	Machine Learning
CNN	Convolutional Neural Network	MMG	Multi-Microgrid
DER	Distributed Energy Resource	MV	Medium Voltage
DL	Deep Learning	NN	Neural Network
ESS	Energy Storage System	NPV	Net Present Value
GHG	Greenhouse Gas	NLP	Nonlinear Programming
GI	Geographic Information	PCC	Point of Common Coupling
GIS	Geographical Information Systems	pdf	probability distribution function
GBM	Geometric Brownian Motion	RES	Renewable Energy Source
EV	Electric Vehicle	RoI	Region of Interest
LV	Low Voltage	SI	Solar Irradiance
Mask R-CNN	Mask Region-Based Convolutional Neural Networks	SOC	State of Charge
MCS	Monte Carlo Simulations	SSLP	Simple Stochastic Linear Programming
MG	Microgrid	TSSP	Two-Stage Stochastic Programming
MILP	Mixed Integer Linear Programming		

also be used for determining solar energy potential, and is therefore used along with solar photovoltaic generation modeling in [13, 14, 15, 16] to estimate the rooftop solar photovoltaic potential for various locations around the world. Furthermore, GIS tools are used in [12] and [17] to determine suitable regions for solar energy development in India and Zambia, respectively.

GIS-based tools can also be used for different aspects of power systems planning. For example, in [18] and [19], GIS tools are used to identify optimal routes for transmission lines at minimum investment cost, while guaranteeing the security of the system. Similarly, a method is proposed in [20] for determining the optimal routing of Medium Voltage (MV) distribution networks in sparse rural areas using GIS, genetic algorithms, and Dijkstra's shortest path algorithm. In [21] and [22], GIS tools and clustering techniques are used to assist in substation expansion planning, while the distribution systems planning problem is addressed in [23] and [24].

The use of GIS for the planning of MGs has also been discussed in the literature. For instance, in [25], a methodology for the optimal formation of MMG systems, considering spatial characteristics, is presented. Similarly, in [26], GIS tools are used for the optimal sizing and allocation of DERs in MGs. In [27], nighttime satellite imagery and census data are used to estimate the size and structure of MGs in rural areas. Similarly, in [28], a framework is presented for forming and clustering Low Voltage (LV) distribution networks to create MMG systems, considering electrical, economic, and geographical constraints with minimum cost.

It can be observed that the aforementioned planning approaches are based on topological considerations, not giving much attention to the geographical characteristics of the MGs locations, leading to inaccuracies or unpractical planning results. In addition, when the location of many elements of the network is unknown or overlooked, the results may be feasible from an optimization viewpoint but not possible to implement. Hence, it has been observed that GIS can assist in finding not only feasible, but realistic areas for the installation of transmission lines, substations, transformers, and protection equipment. The use of Geographic Information (GI) and GIS tools has been also extended to consider the planning of RESs, with the practical application of the results obtained from planning models, especially in locations with limited space, where buildings are in close proximity to each other, which is the case of many Distribution Systems (DSs) and ADNs. In this context, it is important to highlight the possibility of extracting or validating information over imagery, through the use of GIS, while applying GI-based parameters to improve the solution of the optimization problems. These tools are used in this paper in the proposed approach for the planning of MMGs, as discussed in more detail next.

The aforementioned discussion highlights the need to consider the spatial characteristics of the Region of Interest (RoI) in MG and MMG planning. However, GIS have not been widely applied in the literature to identify the RES potential in residential ADNs with the intention of forming MMG systems, while considering the coordination among MGs and the ADN. Thus, GIS tools along with Deep Learning (DL) techniques are used in this paper to accurately model the MV/LV ADN using high-resolution satellite imagery to define the actual RES availability to plan an MMG system. Therefore, the methodology illustrated in Figure 1 is proposed to obtain the capacities of DERs and their time of installation, using parameters obtained applying GIS tools and Machine Learning (ML) techniques while considering uncertainties associated with demand and RES generation. The primary objectives and contributions of this paper are then the following:

- Extend the MMG long-term multi-year planning model proposed in [29] to include the MV and LV grid. The proposed model includes long-term purchase decisions for RES and ESS, long-term transformers capacity selection, short-term operational constraints, and the formu-

Nomenclature

A. Subscripts and Sets

I	Set of RES and ESS capacities $I = \{i\}$
S	Subset of RES $S = \{s\} \in I$
B	Subset of Batteries $B = \{b\} \in I$
t	Subset of LV transformers
b	Battery Type
s	RES type
h	hours
y	years
ω	scenarios

B. Parameters

$\overline{\mathcal{I}}$	Upper limit for solar capacity [kW]
α	Temperature coefficient of power for solar panels [pu/°C]
δ	Depth-Of-Discharge (DOD) of a battery [pu]
η^{Ch}	Efficiency of battery charging [pu]
η^{Dch}	Efficiency of battery discharging [pu]
C	Total number of cycles of charge and discharge of a battery
$\mathcal{H}$	Hours in a year [h]
$\mathcal{M}$	A very large number
$\mathcal{R}$	Capacity of RES [kW] or battery [kWh]
$\overline{\mathcal{I}}_m$	Upper limit for installed capacity of RESs [kW]
$\overline{G}$	Maximum incident SI on solar panels [kW/m^2]
$\overline{P}_{PCC}$	Upper limit for the power flow at the PCC [kW]
τ	Solar cell temperature [°C]
τ_{stc}	Solar cell temperature at standard test conditions [°C]
θ_j	Weight of the jth statistical property of interest for MM approach
φ	Derating factor of solar panels [pu]
c	NPV of O&M costs for RESs or batteries [$/kWh]
d	Discount rate [pu]
e_m	NPV of cost of energy sold by MG "m" [$/kWh]
e_n	NPV of cost of energy purchased from MG "n" [$/kWh]
e_q	NPV of cost of energy purchased from the ADN [$/kWh]
G	Incident SI on solar panels [kW/m^2]
G_{stc}	Incident SI on solar panels at standard conditions [kW/m^2]
K	NPV of unit cost of RES [$/kW] or battery [$/kWh]
P^d	Power demand [kW]
t^{ch}	Time duration a battery can charge continuously at a fixed power [h]
t^{dch}	Time duration a battery can discharge continuously at a fixed power [h]

C. Variables

$\mathcal{A}$	Capacity addition of RESs [kW] or batteries [kWh]
$\mathcal{I}$	Total installed capacity of RESs [kW] or batteries [kWh]
$\mathcal{N}$	Number of types of RESs or batteries considered
C	NPV of capital costs for the MMG system [$]
E^{buy}	Total power purchased by the MMG system [kW]
E^{sell}	Total power sold by the MMG system [kW]
O^B	NPV of O&M costs of batteries for the MMG system [$]
O^S	NPV of O&M costs of solar panels for the MMG system [$]
P'^r	Power received by a MG from the ADN [kW]
P'^s	Power sent by a MG to the ADN [kW]
P^{ch}	Battery charging power [kW]
P^{dch}	Battery discharging power [kW]
P^r	Power received by a MG from other MGs [kW]
P^s	Power sent by a MG to other MGs [kW]
P_s	Power generated by solar panels [kW]
SOC	Battery state-of-charge [kWh]
T	LV transformer capacity [kW]
u'^s, u'^r	ON/OFF state for sending/receiving power to/from the ADN
u^{ch}, u^{dch}	ON/OFF state of battery charging or discharging
u^s, u^r	ON/OFF state for sending/receiving power to/from an MG

lation of the energy transactions among all participants, i.e., among the independent MGs and between each MG and the ADN, while considering spatial characteristics of the MV and LV grid and of the RoI.

- Propose a methodology to estimate the details of the MV and LV ADN using GIS tools, and define the number of users connected to each MV/LV transformer inside the MMG system, using DL techniques over high-resolution

satellite imagery to identify the rooftops of the buildings to determine the actual available solar capacity.

- Test and validate a detailed Two-Stage Stochastic Programming (TSSP) planning model in a real system comprised of four MGs within the ADN of a municipality in the state of São Paulo Brazil, comparing the results of the proposed planning model against the simpler model presented in [29] and Monte Carlo Simulations (MCS), and highlighting the accuracy and computational efficiency of the proposed approach and the benefits of utilizing GIS tools for MMG planning.

The rest of the paper is organized as follow: In Section II, the background and theoretical framework on which the presented work is based are reviewed. In Section III, the optimization model proposed for the long-term planning of MMGs considering the MV/LV grid is explained, as well as the application of GIS tools to include georeferenced parameters in the proposed planning model. In Section IV, the case study and all required input data to apply the model to an ADN grid are introduced, and numerical results are presented, discussed, and compared with respect to a previously proposed planning model. Finally, the main contributions and conclusions of the presented work and possible future research directions are highlighted in Section V.

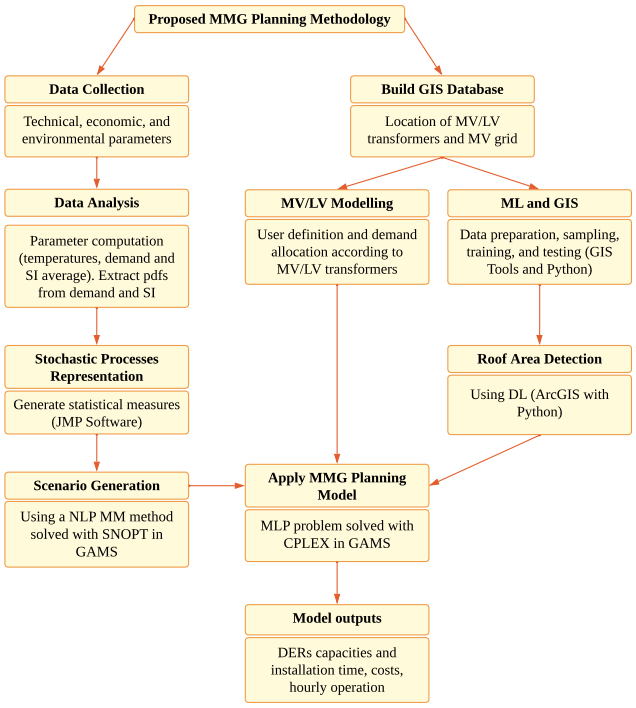


Figure 1: Proposed methodology for the planning of MMG systems.

2. Background

2.1. Multi-Microgrid Planning

An MMG system can be defined as a cluster of independent MGs, where each MG is connected to the ADN through a single Point of Common Coupling (PCC), as depicted in Figure 2. In this context, each MG is managed by its own controller, while the central controller coordinates the connection among MGs and the ADN, so that the electricity demand can be satisfied by DERs within each MG and by the ADN. These attributes, along with different types of constraints representing technical, financial, legal, social, geographical, and environmental conditions are considered in the planning of MMG systems. Therefore, an MMG planning model can be posed as an optimization problem, where an objective function is minimized or maximized, and a set of constraints are considered to decide on the installation/upgrades of new/existing equipment such as RESs and ESSs [30, 31].

The decisions on the capacities needed to satisfy the MMG system's demand are non-anticipative in nature, i.e., these decisions are made "here and now" without the knowledge of the associated uncertainties. On the other hand, the operating decisions are anticipative, i.e., as a "wait and see" response to the observed uncertainty outcomes. Therefore, a TSSP approach is used in this paper for the MMG planning, as it combines the aforementioned requirements efficiently, since this method allows making decisions in two stages, with the objective function including the first stage function (non-anticipative) and the expected value of the second stage function (anticipative). For the MMG problem, as explained in [29], the purchase decisions are assumed to happen in the first stage, whereas the operation of the MMG system belongs to the second stage of the problem.

When applying the TSSP approach, in order to build the scenarios (scenario tree) with their respective probabilities, i.e., random variables that are approximated by discrete probability distribution functions (pdfs), it is important to consider that the associated uncertainties are assumed to be stationary. Thus, the uncertainties associated with RESs can be handled using their inherent statistical properties, whereas the uncertainties related to electricity demand can be considered using Geometric Brownian Motion (GBM), since demand evolves with time and there is an underlying annual growth rate relative to previous years [32, 33]. Once the stochastic processes have been represented, an Moment Matching (MM) approach is used to generate the scenario tree, which is data-driven and thus systematically generates scenarios considering relevant statistical measures, as follows:

$$\begin{aligned} \min_{x,p} \quad & \sum_{j} \theta_j \Big(f_j(X,P) - S_{VAL_j} \Big)^2 \\ \text{s.t.} \quad & \sum_{j \in S} p_s = 1, \\ & p_s \geq 0 \end{aligned} \tag{1}$$

where S is the set of all specified statistical properties j, and S_{VAL_j} is the specified value for the jth statistical property in

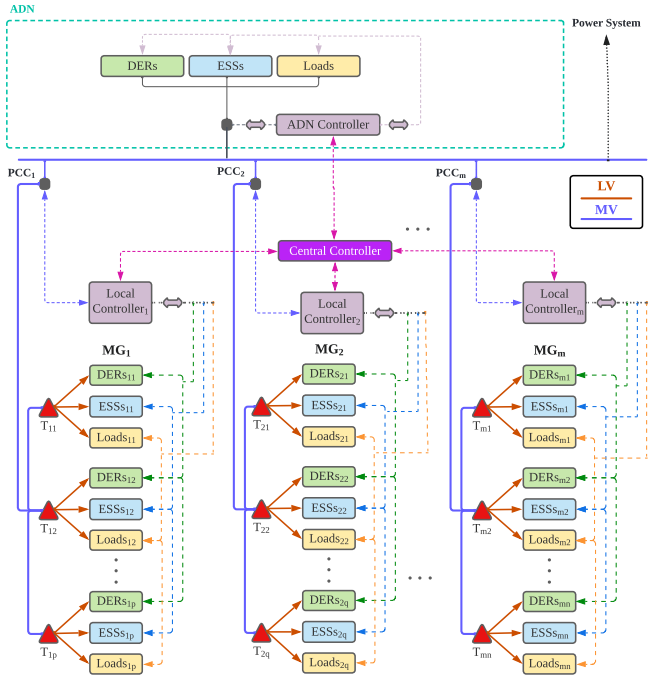


Figure 2: General overview of an MMG system considering the MV/LV distribution network architecture [6].

terms of the original random variables. X represents a single pair of representative values of the uncertainties, i.e., demand and RES, and P represents the associated probabilities; $f_j(X, P)$ is the mathematical discrete expression of the jth statistical property of interest, computed for X and P; and θ_j denotes the weight for the jth statistical property.

2.2. Geographical Information Systems (GIS)

A GIS is a computer-based information system containing a geographical database, which facilitates analysis, modeling, and display of GI for solving complex research planning problems [10]. A modern GIS has at least three main capabilities: (1) GI data management by means of layers that contain the features of the system; (2) spatial analysis tools allowing spatial regressions, distance optimization analysis, population and land use identification, among others; and (3) decision-making awareness for planning and O&M [10]. GI data have two main components: a spatial description of the location or spatial distribution of a geographical phenomenon, and a set of attributes describing the properties of the geometrical data [10]. This data can be organized and displayed using maps, which are instruments to communicate, calculate, and understand the interrelation of real-world features, using locations and attributes [34]. Satellite imagery allows to define the RoI and is based on remote sensing, containing data acquired from the electromagnetic energy reflected by the earth's surface at different spectral wavelengths. This type of imagery can be placed on top of maps at different locations, as in Figure 3, in order to perform quantitative analysis of the RoI based on GIS. Therefore, taking advantage of the detail that high-resolution imagery can offer and the availability of GIS tools, specific characteristics within the RoI such as rooftops can be identified by applying proper classification techniques, which is useful for the planning of MMG systems.



Figure 3: Topological map versus high-resolution imagery of the municipality in the state of São Paulo, Brazil studied in this paper.

3. Planning of MMG Systems

3.1. Multi-Microgrid Planning Model

The model presented in this paper is an extension of the one presented in [29], which has been extensively validated using sensitivity analysis and comparing its results with those obtained with Simple Stochastic Linear Programming (SSLP) and MCS approaches. In this extended model the MV/LV grid is incorporated, as depicted in Figure 2. Therefore, the sub-index t is introduced here to model these elements of the network, assuming RES and ESS capacities within each MG are distributed among the MV/LV transformers, i.e., these are sized from the point of view of the MV/LV transformers (downstream). The model is used to plan the capacities of RESs and ESSs, and the size of MV/LV distribution transformers required to satisfy the hourly demand of an MMG system over the planning horizon, with the exact location being determined during the development/installation stage based on the obtained capacities. In this

model, for every year, battery capacities are included using integer variables, and solar capacities are included using continuous variables, to allow power fractions to be added, as happens in practice. Furthermore, binary variables are used to represent the hourly charging and discharging status of batteries, and power transactions between the participant MGs and the ADN. The size of the MV/LV transformers, RESs, and ESSs is specified using integer variables, while the variables representing the power generation, batteries charge, discharge and hourly State of Charge (SOC), and the power transactions are continuous. Thus, the model can be characterized as a Mixed Integer Linear Programming (MILP) problem based on the identification of the location of the transformers using GIS tools and techniques described below. The capital cost of the MV/LV transformers is not considered here, without loss of generality, so that the results of applying the model can be directly compared to those obtained with [29]. Thus, the intention of the model is to define the minimum required capacity for the transformers to supply demand, while focusing on the introduction of DERs within ADNs to allow MMG system's operation.

The objective function of the model is based on [29] and is formulated as the summation of the discounted, i.e., Net Present Value (NPV), of the capital costs (first stage objective function) and the expected discounted Operation and Maintenance (O&M) and energy transaction costs (second stage objective function) of different stochastic scenarios (ω), as follows:

$$Z = C + \sum_{\omega} (O^{B}_{\omega} + O^{S}_{\omega} + E^{buy}_{\omega} - E^{sell}_{\omega}) p_{\omega} \tag{2}$$

where the discounted capital cost, discounted O&M cost for RESs and batteries, and the discounted cost of the energy purchased and sold are given, respectively, by:

$$C = \sum_{i,y,m,t} K_{i,y} \mathcal{A}_{i,y,m,t} \tag{3}$$

$$O^{S}_{\omega} = \lambda \sum_{s,y,h,m,t} (c_{s,y,m} P_{s,y,h,m,t,\omega}) \quad \forall \omega \tag{4}$$

$$O^{B}_{\omega} = \lambda \sum_{b,y,h,m,t} c_{b,y,m} (P^{ch}_{b,y,h,m,t,\omega} + P^{dch}_{b,y,h,m,t,\omega}) \quad \forall \omega \tag{5}$$

$$E^{buy}_{\omega} = \lambda \sum_{y,h,m} \Big(\sum_{n} P^{r}_{y,h,m,n,\omega} e_{n} + P'^{r}_{y,h,m,\omega} e_{q} \Big) \quad \forall \omega \tag{6}$$

$$E^{sell}_{\omega} = \lambda \sum_{y,h,m} e_{m} \Big(\sum_{n} P^{s}_{y,h,m,n,\omega} + P'^{s}_{y,h,m,\omega} + P^{d}_{y,h,m,\omega} \Big) \quad \forall \omega \tag{7}$$

where factors $\lambda = 30$ and $\mathcal{H} = 288$ are used to carry out the calculations over the whole year, $\mathcal{H}$ is the total number of representative hours in a year, i.e., $24 \times 12 = 288$ hours, based on a 24-hours average day for each of the 12 months, and λ indicates the representative number of days in a month, as per [29]. The units of each parameter and variable, for this and the following definitions and equations, are provided in the Nomenclature section. The necessary constraints for the formulation of the optimization problem are explained next.

3.1.1. Installed Capacity

RES and ESS capacities within each MG are considered to be distributed among the MV/LV transformers. Thus, the total annual installed capacity is determined by updating the total installed capacity of the previous year, as follows:

$$\mathcal{I}_{i,y,m,t} = \mathcal{A}_{i,y,m,t} + \mathcal{I}_{i,y-1,m,t} \quad \forall i, y, m, t \tag{8}$$

where the yearly capacity additions are proportional to the product of the number of generators added each year and their respective individual rated capacity, as follows:

$$\mathcal{A}_{i,y,m,t} = \mathcal{N}_{i,y,m,t} \mathcal{R}_{i} \qquad \forall i, y, m, t \tag{9}$$

The capacity of solar panels is limited by the usable area roofs of the houses inside each MG, as follows:

$$\sum_{y,t} \mathcal{A}_{s,y,m,t} \leq \overline{\mathcal{I}}_{m} \qquad \forall s, m \tag{10}$$

Note that RES power from wind is not considered in the model, as wind turbine deployment in urban areas is unlikely as of now. However, such RES can be easily included in the model if needed.

3.1.2. Supply-Demand Balance

The total demand in the MMG system is equal to the summation of the MG consumer's demand, the batteries storage charge, the power sold to other MGs, and the power sold to the ADN. This demand should be satisfied by the summation of the power generated by RESs, batteries storage discharge, the power received from other MGs, and the power received from the ADN, as follows:

$$\sum_{S,t} P_{s,y,h,m,t,\omega} + \sum_{B,t} P^{dch}_{b,y,h,m,t,\omega} + P^{r}_{y,h,m,\omega} + P'^{r}_{y,h,m,\omega} = \sum_{t} P^{d}_{y,h,m,t,\omega} + \sum_{B,t} P^{ch}_{b,y,h,m,t,\omega} + P^{s}_{y,h,m,\omega} + P'^{s}_{y,h,m,\omega} \quad \forall y, h, m, \omega \tag{11}$$

where the power received/sold from/to other MGs are defined as follows:

$$P^{r}_{y,h,m,\omega} = \sum_{n} P^{r}_{y,h,m,n,\omega} \qquad \forall y, h, m, \omega \tag{12}$$

$$P^{s}_{y,h,m,\omega} = \sum_{n} P^{s}_{y,h,m,n,\omega} \qquad \forall y, h, m, \omega \tag{13}$$

with $P^{r}_{y,h,m,n,\omega} = P^{s}_{y,h,m,n,\omega}$ for any specific hour of the planning horizon. In addition, two independent MGs are not allowed to sell/receive power to/from each other at the same time, and any independent MG is not allowed to sell/receive power to/from the ADN at the same time, which is enforced through the following constraints:

$$P^{r}_{y,h,m,\omega} P^{s}_{y,h,m,\omega} = 0 \qquad \forall y, h, m, \omega \tag{14}$$

$$P'^{r}_{y,h,m,\omega} P'^{s}_{y,h,m,\omega} = 0 \qquad \forall y, h, m, \omega \tag{15}$$

3.1.3. Operating Reserves

To guarantee each MG can withstand a failure that may cause their disconnection from the ADN at the PCC, an adequate amount of energy in the batteries should be kept at all times. This is achieved through the following constraint:

$$\sum_{B,t} SOC_{b,y,h,m,t,\omega} \geq \sum_{t} P^{d}_{y,h,m,t,\omega} - \sum_{S,t} P_{s,y,h,m,t,\omega} \quad \forall s, b, h, y, m, \omega \tag{16}$$

3.1.4. Operating Limits

The power that individual MGs can sell to other MGs and the ADN is limited by the available RES power and battery storage discharge, as follows:

$$P^{s}_{y,h,m,\omega} + P'^{s}_{y,h,m,\omega} \leq \sum_{t} (P_{s,y,h,m,t,\omega} + P^{dch}_{b,y,h,m,t,\omega}) \quad \forall s, b, y, h, m, \omega \tag{17}$$

In addition, the limit in the power flow at the PCC is represented as a function of the power transacted at that point, as follows:

$$|(P^{s}_{y,h,m,\omega} + P'^{s}_{y,h,m,\omega}) - (P^{r}_{y,h,m,\omega} + P'^{r}_{y,h,m,\omega})| \leq \overline{P}_{PCC} \quad \forall s, b, y, h, m, \omega \tag{18}$$

Similarly, the capacity of each transformer is limited by its power flow, as follows:

$$|P_{s,y,h,m,t,\omega} + P^{dch}_{b,y,h,m,t,\omega} - P^{d}_{y,h,m,t,\omega} - P^{ch}_{b,y,h,m,t,\omega}| \leq T_{m,t} \quad \forall s, b, y, h, m, t, \omega \tag{19}$$

3.1.5. RESs Output

The power output is computed as a direct function of the hourly incident irradiance, hourly cell temperature, and derating factor, as follows:

$$P_{s,y,h,m,t,\omega} = \varphi \mathcal{I}_{s,y,m,t} \left(\frac{G_{y,h,\omega}}{G_{stc}} \right) [1 + \alpha(\tau_h - \tau_{stc})] \quad \forall s, y, h, m, t, \omega \tag{20}$$

3.1.6. Battery SOC and Limits

For every hour of operation, the batteries' SOC is computed as a function of their charge and discharge power, considering the charging and discharging efficiency rates, as follows:

$$SOC_{b,y,h+1,m,t,\omega} - SOC_{b,y,h,m,t,\omega} = \eta^{ch} P^{ch}_{b,y,h,m,t,\omega} - \frac{P^{dch}_{b,y,h,m,t,\omega}}{\eta^{dch}} \quad \forall b, y, h, m, t, \omega \tag{21}$$

$$SOC_{b,y+1,1,m,t,\omega} - SOC_{b,y,\mathcal{H},m,t,\omega} = \eta^{ch} P^{ch}_{b,y,\mathcal{H},m,t,\omega} - \frac{P^{dch}_{b,y,\mathcal{H},m,t,\omega}}{\eta^{dch}} \quad \forall b, y, h, m, t, \omega \tag{22}$$

The boundaries of the SOC, which reflect the minimum and maximum capacity of the batteries, are computed as follows:

$$SOC_{b,y,h,m,t,\omega} \leq \mathcal{I}_{b,y,m,t} \quad \forall b, y, h, m, t, \omega \tag{23}$$

$$SOC_{b,y,h,m,t,\omega} \geq \delta \mathcal{I}_{b,y,m,t,} \quad \forall b, y, h, m, t, \omega \tag{24}$$

In addition, the following constraints represent the upper limit of the batteries charge and discharge power, which are computed as a function of their Depth-of-Discharge (DOD), total installed battery capacity, and continuous time duration of charging and discharging:

$$P^{ch}_{b,y,h,m,t,\omega} \leq \left(\frac{1-\delta}{t^{ch}} \right) \mathcal{I}_{b,y,m,t} \quad \forall b, y, h, m, t, \omega \tag{25}$$

$$P^{dch}_{b,y,h,m,t,\omega} \leq \left(\frac{1-\delta}{t^{dch}} \right) \mathcal{I}_{b,y,m,t} \quad \forall b, y, h, m, t, \omega \tag{26}$$

Furthermore, the minimum charging/discharging power at a given hour are given by the following constraint:

$$P^{dch}_{b,y,h,m,t,\omega} \geq u^{dch}_{b,y,h,m,t,\omega} \quad \forall b, y, h, m, t, \omega \tag{27}$$

$$P^{ch}_{b,y,h,m,t,\omega} \geq u^{ch}_{b,y,h,m,t,\omega} \quad \forall b, y, h, m, t, \omega \tag{28}$$

The following constraint is used to guarantee that battery charging and discharging do not take place at the same time:

$$P^{dch}_{b,y,h,m,t,\omega} P^{ch}_{b,y,h,m,t,\omega} = 0 \quad \forall b, y, h, m, t, \omega \tag{29}$$

Finally, the following constraint defines the life span of each battery for C cycles of charge and discharge:

$$\sum_{h,y} (P^{ch}_{b,y,h,m,t,\omega} + P^{dch}_{b,y,h,m,t,\omega}) \leq C \sum_{y} \mathcal{A}_{b,y,m,t} \quad \forall b, m, t, \omega \tag{30}$$

Equations (14), (15), and (29) are nonlinear, and are thus linearized, respectively, as follows [35]:

$$P^{dch}_{b,y,h,m,t,\omega} \leq u^{dch}_{b,y,h,m,t,\omega} \mathcal{M} \quad \forall b, y, h, m, t, \omega \tag{31}$$

$$P^{ch}_{b,y,h,m,t,\omega} \leq u^{ch}_{b,y,h,m,t,\omega} \mathcal{M} \quad \forall b, y, h, m, t, \omega \tag{32}$$

$$u^{dch}_{b,y,h,m,t,\omega} + u^{ch}_{b,y,h,m,t,\omega} \leq 1 \quad \forall b, y, h, m, t, \omega \tag{33}$$

$$P^{s}_{y,h,m,\omega} \leq u^{s}_{y,h,m,\omega} \mathcal{M} \quad \forall y, h, m, \omega \tag{34}$$

$$P^{r}_{y,h,m,\omega} \leq u^{r}_{y,h,m,\omega} \mathcal{M} \quad \forall y, h, m, \omega \tag{35}$$

$$u^{s}_{y,h,m,\omega} + u^{r}_{y,h,m,\omega} \leq 1 \quad \forall y, h, m, \omega \tag{36}$$

$$P^{s'}_{y,h,m,\omega} \leq u^{s'}_{y,h,m,\omega} \mathcal{M} \quad \forall y, h, m, \omega \tag{37}$$

$$P^{r'}_{y,h,m,\omega} \leq u^{r'}_{y,h,m,\omega} \mathcal{M} \quad \forall y, h, m, \omega \tag{38}$$

$$u^{s'}_{y,h,m,\omega} + u^{r'}_{y,h,m,\omega} \leq 1 \quad \forall y, h, m, \omega \tag{39}$$

where $\mathcal{M}$ is a large number used to ensure redundancy if the associated binary variable becomes 1. Similarly, nonlinear equations (18) and (19) are replaced, respectively, by the following set of linear equations:

$$(P^{s}_{y,h,m,\omega} + P'^{s}_{y,h,m,\omega}) - (P^{r}_{y,h,m,\omega} + P'^{r}_{y,h,m,\omega}) \leq \overline{P}_{PCC} \quad \forall y, h, m, \omega \tag{40}$$

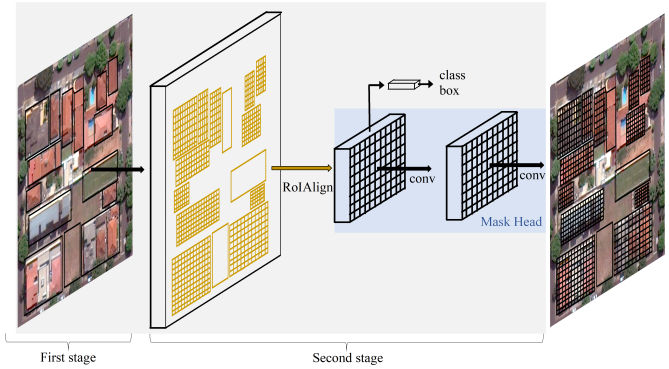


Figure 4: Mask R-CNN framework for instance segmentation applied to rooftop identification for installation potential of solar PV [38].

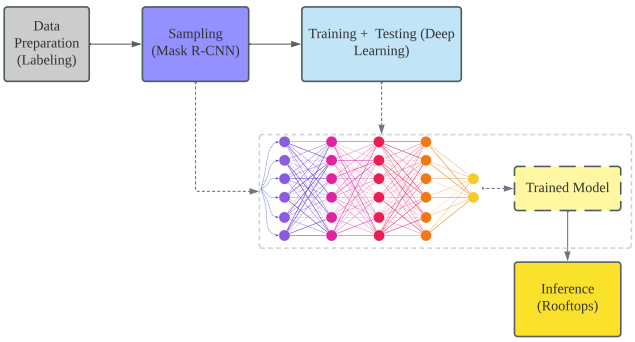


Figure 5: DL Framework for detecting rooftops.

$$-(P^{s}_{y,h,m,\omega} + P'^{s}_{y,h,m,\omega}) + (P^{r}_{y,h,m,\omega} + P'^{r}_{y,h,m,\omega}) \leq \overline{P}_{PCC} \quad \forall y, h, m, \omega \tag{41}$$

$$(P_{s,y,h,m,t,\omega} + P^{dch}_{b,y,h,m,t,\omega}) - (P^{d}_{y,h,m,t,\omega} + P^{ch}_{b,y,h,m,t,\omega}) \leq T_{m,t} \quad \forall s, b, y, h, m, t, \omega \tag{42}$$

$$-(P_{s,y,h,m,t,\omega} + P^{dch}_{b,y,h,m,t,\omega}) + (P^{d}_{y,h,m,t,\omega} + P^{ch}_{b,y,h,m,t,\omega}) \leq T_{m,t} \quad \forall s, b, y, h, m, t, \omega \tag{43}$$

3.2. DER and LV Network Identification Through GIS Tools

DL is a ML technique where knowledge is extracted from a structured dataset, allowing models of multiple processing layers to learn and represent data with multiple levels of abstraction [36, 37]. One of the main applications of DL is computer vision, which is dedicated to interpreting and understanding images and video [37]. These techniques are used here to identify the rooftops in the RoI for PV deployment potential.

Image segmentation, which is the precise delineation of objects in an image, uses traditional object vision to localize and classify objects using bounding boxes, and semantic segmentation to classify each pixel into a predefined set of categories [38]. Thus, image segmentation can be used to detect building footprints, which is very useful for defining the potential areas for PV installation. There are different models for image segmentation, and their applicability depends on the purpose of the study, characteristics of the RoI, and information availability. Thus, in this paper, since the buildings in the RoI are very close to each other, the Mask Region-Based Convolutional Neural Networks (Mask R-CNN) method is used [39].

Mask R-CNN, depicted in Figure 4, is a specialized kind of Neural Network (NN) that can be employed to process data with a known grid-like topology such as image data, which can be considered a 2-D grid of pixels [36]. Mask R-CNN predicts object class and bounding boxes in two stages. The first stage, which consists of two NNs (backbone and Region Proposal) is to propose candidate object bounding boxes, while the second stage extracts features from each candidate box and performs classification, predicting in parallel segmentation masks, i.e., the desired features on each RoI.

3.2.1. Solar PV Potential

As mentioned, building footprints can be detected using DL, which leads to defining available rooftop areas for solar panel installation. In this paper, this workflow is carried out in ArcGIS Pro over high-resolution imagery, following the steps presented in Figure 5. This process includes: data *preparation* by creating labels of the elements to be detected; *samples* creation using Mask R-CNN format for training and testing; and *inference* to generate bounding boxes over the RoI on the high-resolution imagery. For the Mask R-CNN approach, RestNet50 is used as the backbone/feature extracting NN, which contains 50 layers (48 Convolutional Neural Network (CNN), 1 Max Pool, 1 Average Pool), and a Regional Proposal Network with 3 layers. Thus, the maximum solar generation availability $\overline{I}$ in kW can be defined as a function of the available rooftop area A in m^2, peak Solar Irradiance (SI) $\overline{G}$ in kW/m^2, and solar panels efficiency η in p.u., as follows:

$$\overline{I}_m = A \times \overline{G} \times \eta \tag{44}$$

3.2.2. MV/LV Network Modeling

A methodology is proposed here to obtain an approximate representation of the MV/LV grid in an MMG system. Thus, assuming the LV network is unknown, but the location of the MV/LV transformers is given, the LV network can be outlined by identifying the number of users connected to each transformer. This number can be further utilized to divide each MG's hourly demand proportionally, allowing the representation of the hourly demand at each transformer. This is achieved considering that one or more transformers divide each MG in a series of blocks, as depicted in Figure 6. Therefore, cadastral information can be used to define the distribution of the users among all the transformers for all the MGs. If this information is not available, 3D imagery or web-based map services can be used as an alternative.

4. Simulations and Results

4.1. Case Study

In this study case, the DL methodology described in Section 3.2.1 is used to define the solar generation availability over

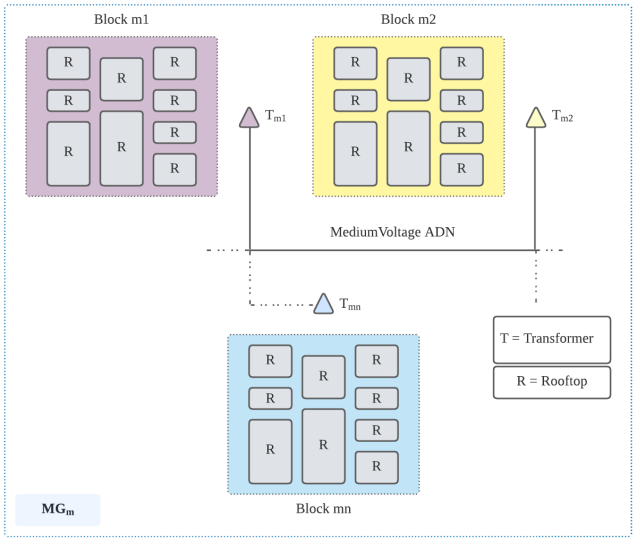


Figure 6: Methodology to estimate the number of users for each MV/LV transformer.

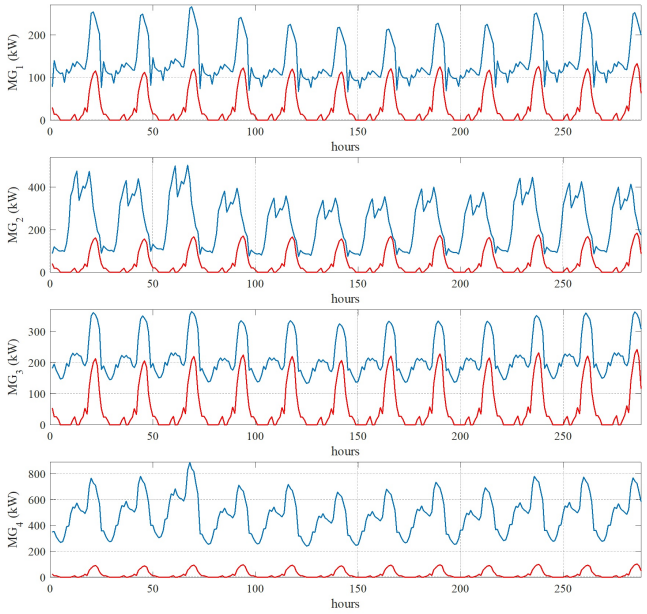


Figure 7: MG growing demand in blue and fixed demand (EVs) in red [29].

the RoI, an ADN in a municipality in the state of São Paulo, Brazil. The methodology presented in Section 3.2.2 is used to define the number of users located at each MV/LV transformers. These parameters are introduced in the planning model presented in Section 3.1, which is used to study the feasibility of implementing an MMG system consisting of 4 individual MGs. All the input data, including technical, economic, and environmental parameters used for this case study are discussed next.

4.1.1. Region of Interest (RoI)

A four-band (RGBN)[1]/multi-spectral high-resolution satellite imagery[2] for the studied municipality is used, as recommended in [40].

4.1.2. Electricity Demand

The hourly average demand of a year for the required 288 representative hours, as discussed in Section 3.1, is presented in Figure 7 for the 4 identified MGs. The load has been divided into two parts: growing and fixed, in which the fixed demand is assumed to represent Electric Vehicle (EV) demand [29].

4.1.3. Solar Panels

The rooftop solar panels are assumed to be connected through an inverter located at each house. Also, for each MG, all the rooftop solar panels connected downstream from each MV/LV transformer are assumed to be lumped at the corresponding transformer. Hourly data for SI and ambient temperature are synthetically generated using PVsyst software considering statistical and meteorological constraints [41]. The cell temperature, which is the temperature of the surface of the PV array, is computed considering the ambient temperature and other manufacture parameters, according to [42]. Thus, average SI and cell temperature are used to compute the power output, as shown in Figure 8, using (20) as per [29]. The operational parameters and costs associated with the panels, with a lifetime of 20 years, are shown in Table 1.

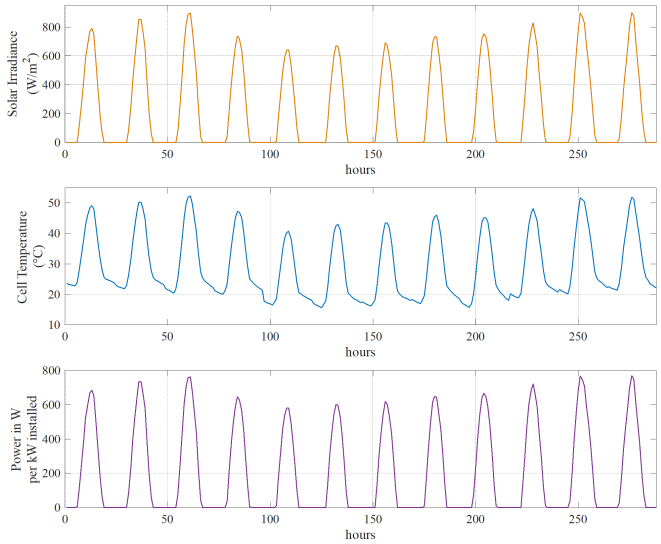


Figure 8: Average SI, cell temperature, and resulting power availability in W per kW installed for a municipality in the state of São Paulo, Brazil [43].

[1]Four band imagery typically contains red, green, blue, and near-infrared bands. Only three bands can usually be viewed at one time in most software applications, and the imagery's natural color (red, green, and blue bands) is used for this application

[2]The high-resolution imagery was purchased from Satellite Imaging Corporation, Houston, TX (www.satimagingcorp.com).

Table 1: Solar panels parameters [29]

$K_{s,1,m}$ $\forall m$ ($/kW)	$c_{s,1,m}$ $\forall m$ ($/kWh)	α (pu/°C)	φ (%)	τ_{stc} (°C)	G_{stc} (kW/m^2)
871	0.002487	-0.041	98	25	1

Table 2: Battery parameters [29]

$K_{b,1,m}$ $\forall m$ ($/kWh)	$c_{b,1,m}$ $\forall m$ ($/kWh)	η_{Ch} (%)	η_{DCh} (%)	Lifetime (Cycles)
654	0.00187	81.6 %	81.6%	10,000

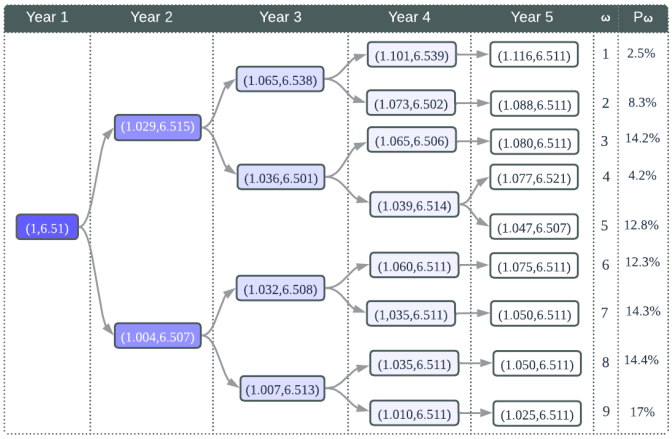


Figure 9: Scenario tree for the planning of MMG in a municipality in the state of São Paulo, Brazil, with a growth factor for variable demand with respect to year 1 and average SI [29].

4.1.4. Batteries

Lithium iron phosphate battery packs with 20 kWh and 8 kW peak power of charge/discharge, i.e., $t^{ch} = t^{dch} = 2h$ with $\delta = 0.2$, are used for the case study. Additional technical and economic parameters for the batteries are presented in Table 2, where the capital cost yields 1,380 $/kW, as per [29].

4.1.5. Stochastic Scenarios

The scenarios used for this paper were generated using an MM approach, as explained in Section 2.1 and discussed in detail in [29], where the expected value $\mathbb{E}$, variance $\mathbb{V}ar$, and skewness sk are the statistical measures considered for each uncertain value. It was observed that, to avoid under- and over-specification, the number of scenarios should be at least equal to the total number of statistical measures plus one degree of freedom. Therefore, in this case study, the 9-scenario tree presented in Figure 9 is used, as per [29], which at each node indicates the demand growth rate with respect to year 1 and the SI annual average, for a 5-year planning horizon, with their respective probabilities.

4.2. Assumptions

The following assumptions are considered in the study case:

4.2.1. Solar Generation Availability

The analysis was performed in ArcGIS Pro in a computer with two Intel Xenon Silver 4214 processors at 2.20 GHz, 512 GB ram memory, and NVIDIA RTX A5000 GPUs. For this case study, 10,000 samples have been considered, of which 90% were used for training and 10% were used for validation. The batch size, which is the number of image tiles to be processed for training is 4; the chip size, which sets the image size to train the model is 400 pixels; and the maximum epoch, which indicates the number of times the data set is passed forward and backward through the NN, is set to 20 [39]. The training process yielded an optimal learning rate between $5.24x10^{-5}$ and $5.24x10^{-6}$, which was extracted from the learning curve. Furthermore, it is assumed that 75% of the total rooftop area is suitable for solar panels installation, considering the roof characteristics in the RoI. Also, a maximum SI of 722 kW/m^2 and a 20% efficiency for solar panels are considered.

4.2.2. MMG Planning

The MILP model, described in Section 3.1 was solved using GAMS, with the CPLEX solver in a computer with Intel Xeon CPU at 1.87 GHz. In this case study, at least 10% of the maximum available capacity of solar generation should be included for each transformer, at each MG, otherwise the model does not include them due to the cost minimization approach and low grid electricity costs. The remaining model parameters are presented in Table 3.

Table 3: Model parameters

Discount rate d	8%
Electricity price growth	4.81%/year
O&M costs increase	3%/year (average inflation)
Solar panels cost decrease	9%/year
Batteries cost decrease	21.1%/year
MCS convergence	700 iterations
PCC power limit $\overline{P}_{PCC}$	1200 kW
Electricity Prices	$(e_a = e_l = e_m)$ $/kWh 0.11 for $h = 17$ (intermediate) 0.17 for $18 < h \leq 20$ (peak) 0.08 otherwise (off-peak)

4.3. Numerical Results

The results of the MMG planning model for the aforementioned ADN using the TSSP approach are first compared with the MCS results, which are considered as a benchmark for the case study. The results of the TSSP model presented in this paper are also compared with the ones obtained with the simpler TSSP model presented in [29], based on the same solar PV limits obtained here.

4.3.1. Solar Generation Maximum Capacities

The DL methodology described in Section 3.2 is used to identify the rooftops of the buildings within the RoI. The training of the DL model was completed in 134 hours and 28 min-

utes, with Figure 10 depicting both the training loss and validation error decreasing over time, and thus showing a good fit, with an average precision score of 89.2%. The trained model allows to identify the rooftop areas for each MG, as depicted in Figures 11 to 14. Using these areas, the solar power maximum capacity for each MG is calculated using the methodology described in Section 3.2.1, and the results are presented in Table 5.

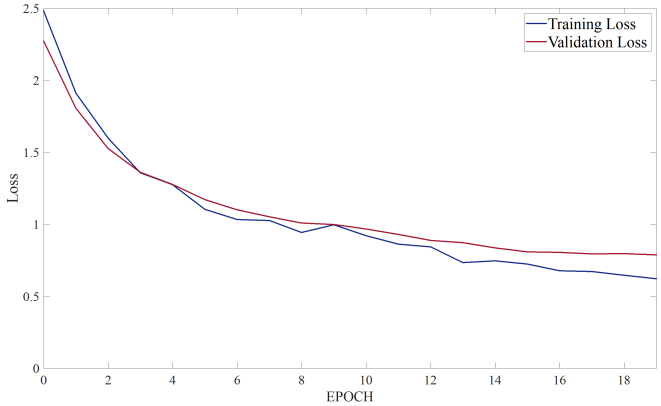


Figure 10: Loss graph of training of the DL model.

4.3.2. Number of Users

To estimate the number of users connected to each MV/LV transformer, the methodology presented in Section 3.2.2 is applied, which includes the use of the areas detected in Section 4.3.1, web-based map services, and some public cadastral information. In addition, it was assumed that a certain number of EVs can be adopted within each MG, based on existing vehicle data. The number of estimated users and EVs are depicted in Table 5.

Table 4: Total cost and computational cost

Model	Total Costs (M$)	Computational Costs (hh:mm:ss)
MCS	1.95	632:00:00
TSSP [29]	1.87	03:16:44
TSSP	1.89	46:25:31

4.3.3. MMG Planning

The results of the TSSP planning model are presented in Tables 4, 6, and 7. The results in Table 4 show that the total cost of the TSSP model is consistently close to the benchmark. In fact, the total cost in the TSSP model is only 3.07% lower than the one obtained with MCS. However, the TSSP model is much faster than the MCS for the large planning problem considered here due to its level of granularity.

The solar generation capacities obtained from the different models are shown in Table 6, which shows that all of them yield the same results for the size and location of solar panels since as previously explained, RES requirements have to be forced

Table 5: Number of users and EVs, rooftop area associated with each transformer, and RES limits

MG_1				
$T_{1,t}$	EVs	Users	Area (m^2)	RES max. capacity (kW)
1	-	12	1955	212
2	-	28	4970	539
3	2	29	3423	371
4	5	31	4659	505
5	-	22	4230	458
6	1	21	3962	429
7	7	28	3829	415
8	3	27	4262	462
9	-	23	4828	523
MG_2				
$T_{2,t}$	EVs	Users	Area (m^2)	RES max. capacity (kW)
1	9	43	4477	485
2	-	18	3654	396
3	2	21	2011	218
4	-	21	2011	218
5	-	35	3442	373
6	2	19	3309	359
7	5	32	631	68
8	-	10	1951	211
9	5	14	2091	227
10	-	24	989	107
MG_3				
$T_{3,t}$	EVs	Users	Area (m^2)	RES max. capacity (kW)
1	-	36	4179	453
2	2	25	3835	416
3	3	18	3512	381
4	17	65	3071	333
5	3	22	3947	428
6	-	35	3128	339
7	3	24	4656	505
8	5	23	4341	470
MG_4				
$T_{4,t}$	EVs	Users	Area (m^3)	RES max. capacity (kW)
1	2	25	2147	233
2	2	16	1331	144
3	3	20	2033	220
4	4	13	1186	128
5	3	16	2208	239



Figure 11: Blocks, rooftops, transformers, and MV grid corresponding to MG1.

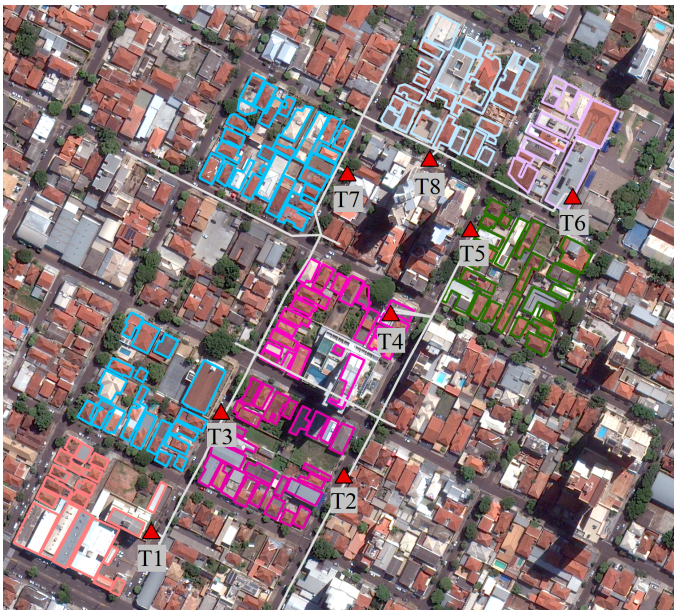


Figure 13: Blocks, rooftops, transformers, and MV grid corresponding to MG3.



Figure 12: Blocks, rooftops, transformers, and MV grid corresponding to MG2.



Figure 14: Blocks, rooftops, transformers, and MV grid corresponding to MG4.

into the model. The batteries obtained with both TSSP models are very similar, with the standard deviation of the difference in the capacity installed for each independent MG (Table 7) with respect to the MCS benchmark being 10.1 % or 16.7 kWh in average, which is relatively small, thus validating the TSSP approaches.

In Figure 15, the capacity additions for the MMG system obtained with the TSSP are shown. Note that all the solar panels and 93.5% of the battery capacities are installed at the beginning of the planning horizon, while the remaining battery capacity is added between the second and fourth year. This is particularly related to Brazilian distribution companies, given the limited-time government incentives for initial investments. In addition, unlike the model presented in [29], the extended model provides more relevant details for decision-making, as the location of solar panels and batteries within the RoI can be obtained. Thus, providing optimal capacities from economic, technical, and geographical points of view, that can be actually implemented within the RoI. Similarly, by enforcing the solar PV capacity at each transformer through (9), there is a realistic allocation of RES that cannot be obtained with the model presented in [29].

Table 6: Total solar installed capacities for the MMG system, for TTSP and MCS

TSSP and MCS with MV/LV				
t	MG_1 (kW)	MG_2 (kW)	MG_3 (kW)	MG_4 (kW)
1	21	49	45	23
2	54	40	42	14
3	37	22	38	22
4	50	22	33	13
5	46	37	43	24
6	43	36	34	-
7	41	7	50	-
8	46	21	47	-
9	52	23	-	-
10	-	11	-	-
Total	391	266	332	96
TSSP without MV/LV (kWh/kW)				
Total	391	266	332	96

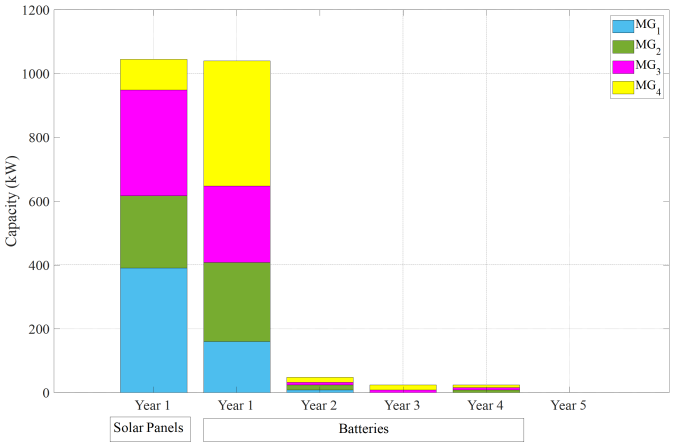


Figure 15: Yearly capacity additions from TSSP model.

The minimum capacity of the MV/LV transformers for the TSSP model and MCS are shown in Table 8, where the average difference in the total transformer capacity required for the MMG system is only 1.47%. In addition, observe that the relationship between each transformer's capacity and the total transformer capacity inside each MG is not related to the number and location of users exclusively, as (18) ensures that the capacity of the transformers accounts for the power of DERs. Note that the location and capacity of these transformers can be used for expansion planning of the complete distribution network.

5. Conclusion

This paper presented a TSSP approach and model for the realistic planning of MMG systems considering uncertainties associated with electricity demand and RES availability. In addition, GIS tools and DL were used to specify the actual rooftop availability for solar panel installation from high-resolution imagery. Thus, GIS tools facilitated the inclusion of georeferenced parameters within the optimization formulation, while allowing the visualization of the results on the real network using maps. This allows the deployment of DERs in the real network since the results clearly show where RES can be physically located. Furthermore, it was shown that GI allows the modelling of the distribution network as the location of the MV distribution network and MV/LV distribution transformers can be properly identified. Finally, the benefits of solving MMG planning problems using TSSP models as opposed to MCS are clearly highlighted, since adequate results can be timely obtained as the size of the problem associated with the level of granularity increases.

To further improve the proposed planning model, power flow equations may be included to validate the operation of the MMG system in the long-term, thus allowing to account for power losses and voltage issues at the PCC and at the MV/LV transformers. In addition, even though in the proposed model, a cost of battery operation is included and its lifetime is accounted for in terms of cycles, which is a widely used approach to indirectly account for battery degradation in long-term planning models, a more detailed modeling of the battery ESS degradation over the total DER capacity and associated costs may be studied.

Table 7: Total batteries installed capacities for the MMG system

MCS with MV/LV (kWh/kW)				
t	MG_1	MG_2	MG_3	MG_4
1	71/29	111/44	125/50	667/267
2	47/19	73/29	60/24	13/52
3	45/18	70/28	58/23	113/45
4	46/18	68/27	63/25	112/45
5	46/19	71/28	54/22	116/46
6	48/19	69/28	70/28	-
7	49/19	71/28	93/37	-
8	51/21	69/27	150/60	-
9	56/22	69/28	-	-
10	-	73/28	-	-
Total	459/184	743/297	667/267	1138/455
TSSP without MV/LV (kWh/kW)[29]				
Total	420/168	660/254	640/256	1080/432
TSSP with MV/LV (kWh/kW)				
t	MG_1	MG_2	MG_3	MG_4
1	60/24	60/24	80/32	300/120
2	40/16	60/24	40/16	220/88
3	40/16	60/24	80/32	160/64
4	40/16	60/24	120/48	200/80
5	60/24	60/24	100/40	200/80
6	20/8	120/48	60/24	-
7	60/24	60/24	60/24	-
8	60/24	60/24	120/48	-
9	40/16	60/24	-	-
10	-	80/32	-	-
Total	420/168	680/272	660/264	1080/432

Table 8: Transformers capacities

MCS (kW)				
t	MG_1	MG_2	MG_3	MG_4
1	41	166	97	455
2	49	54	74	211
3	60	70	67	252
4	81	61	238	187
5	40	88	72	210
6	45	65	82	-
7	92	105	92	-
8	65	41	117	-
9	49	77	-	-
10	-	74	-	-
Total	523	801	839	1316

TSSP (kW)				
t	MG_1	MG_2	MG_3	MG_4
1	40	151	91	362
2	42	51	65	242
3	61	69	80	244
4	74	57	259	211
5	47	83	92	197
6	40	90	79	-
7	104	106	74	-
8	67	38	117	-
9	43	79	-	-
10	-	75	-	-
Total	518	797	855	1256

Acknowledgments

The authors would like to thank Joel D. Melo, Tatiana P. Guedes, and Ahda G. Pavani, researchers from the Federal University of ABC from São Paulo, Brazil for their support and for providing some of the data used in this paper.

References

[1] M. Hafner, M. Noussan, Technologies for the Global Energy Transition, Springer International Publishing, Cham, 2020, pp. 177–202.

[2] H. Farhangi, G. Joos, Microgrid Planning and Design: A Concise Guide, 1st ed., Wiley-IEEE Press, 2019.

[3] Z. Rajab, A. Alfergani, A. Asheibi, A. Khalil, F. Mohamed, Optimum microgrid planning and operation for improving reliability and power quality: Review, in: 2020 11th International Renewable Energy Congress (IREC), 2020, pp. 1–6.

[4] M. Farrokhabadi, C. Canizares, J. W. Simpson-Porco, et al., Microgrid Stability Definitions, Analysis, and Examples, IEEE Transactions on Power Systems 35 (2019) 13–29.

[5] A. Cagnano, E. De Tuglie, P. Mancarella, Microgrids: Overview and guidelines for practical implementations and operation, Applied Energy 258 (2020) 1–18.

[6] B. Chen, J. Wang, X. Lu, C. Chen, S. Zhao, Networked microgrids for grid resilience, robustness, and efficiency: A review, IEEE Transactions on Smart Grid 12 (2021) 18–32.

[7] M. Erol-Kantarci, B. Kantarci, H. T. Mouftah, Reliable overlay topology design for the smart microgrid network, IEEE Network Journal 25 (2011) 38–43.

[8] F. Shahnia, S. Bourbour, A. Ghosh, Coupling neighboring microgrids for overload management based on dynamic multicriteria decision-making, IEEE Transactions on Smart Grid 8 (2017) 969–983.

[9] M. S. Saleh, A. Althaibani, Y. Esa, Y. Mhandi, A. A. Mohamed, Impact of clustering microgrids on their stability and resilience during blackouts, in: 2015 International Conference on Smart Grid and Clean Energy Technologies (ICSGCE), 2015, pp. 195–200.

[10] P. A. Longley, M. F. Goodchild, D. J. Maguire, D. W. Rhind, Geographic Information Science and Systems, 4th ed., Wiley, Hoboken, N.J., 2015.

[11] N. E. Koltsaklis, A. S. Dagoumas, G. M. Kopanos, E. N. Pistikopoulos, M. C. Georgiadis, A spatial multi-period long-term energy planning model: A case study of the greek power system, Applied Energy Journal 115 (2014) 456–482.

[12] T. Ramachandra, B. Shruthi, Spatial mapping of renewable energy potential, Renewable and Sustainable Energy Reviews 11 (2007) 1460–1480.

[13] S. Rhythm, B. Rangan, Estimation of rooftop solar photovoltaic potential of a city, Solar Energy 115 (2015) 589–602.

[14] Z. A. Latif, N. A. M. Zaki, S. A. Salleh, Gis-based estimation of rooftop solar photovoltaic potential using lidar, in: 2012 IEEE 8th International Colloquium on Signal Processing and its Applications, 2012, pp. 388–392.

[15] G. Pieter, M. Robert, M. Jennifer, C. Phillips, E. Ryan, Rooftop Photovoltaic Technical Potential in the United States, Technical Report, NREL, 2019.

[16] V. M. Phap, N. T. Thu Huong, P. T. Hanh, P. Van Duy, D. Van Binh, Assessment of rooftop solar power technical potential in hanoi city, vietnam, Journal of Building Engineering 32 (2020) 101528.

[17] M. Mwanza, K. Ulgen, GIS-Based Assessment of Solar Energy Harvesting Sites and Electricity Generation Potential in Zambia, Springer International Publishing, Cham, 2021, pp. 899–946.

[18] J. Shu, L. Wu, Z. Li, M. Shahidehpour, L. Zhang, B. Han, A new method for spatial power network planning in complicated environments, IEEE Transactions on Power Systems 27 (2012) 381–389.

[19] E. Garcia-Garrido, L. A. Fernandez-Jimenez, M. Mendoza-Villena, P. M. Lara-Santillan, P. J. Zorzano-Santamaria, E. Zorzano-Alba, A. Falces, Electric power distribution planning tool based on geographic information systems and evolutionary algorithms, in: 2017 European Conference on Electrical Engineering and Computer Science (EECS), 2017, pp. 396–401.

[20] J. R. E. Fletcher, T. Fernando, H. H. Iu, M. Reynolds, S. Fani, Spatial optimization for the planning of sparse power distribution networks, IEEE Transactions on Power Systems 33 (2018) 6686–6695.

[21] S. Vahedi, M. Banejad, M. Assili, Gis-based substation expansion planning, IEEE Systems Journal 15 (2021) 959–970.

[22] Z. Quan, S. Caixin, C. Guoqing, D. Qun, L. Ruijin, Gis-based distribution system spatial load forecasting and the optimal planning of substation location and capacity, Proceedings. International Conference on Power System Technology 2 (2002) 885–889.

[23] I. Y. Adejoh, S. A. Samuel, Application of gis in electrical distribution network system, in: European International Journal of Science and Technology, volume 4, 2015.

[24] N. Boulaxis, M. Papadopoulos, Optimal feeder routing in distribution system planning using dynamic programming technique and gis facilities, IEEE Transactions on Power Delivery 17 (2002) 242–247.

[25] S. Xie, H. Wang, S. Wang, H. Lu, Y. Hong, D. Jin, Q. Liu, Discovering communities for microgrids with spatial-temporal net energy, Journal of Modern Power Systems and Clean Energy 7 (2019) 1536–1546.

[26] E. J. Molina Bacca, Optimal Sizing and Geographic Placement of the Components of a Microgrid, Master Thesis. University of Calgary, Schulich School of Engineering (2018).

[27] M. Lugo-Alvarez, R. Broderick, E. I. Ortiz-Rivera, Strategic placement and design of microgrids using nighttime imagery, in: 2020 47th IEEE Photovoltaic Specialists Conference (PVSC), 2020, pp. 1730–1734.

[28] S. Mojtahedzadeh, S. N. Ravadanegh, M.-R. Haghifam, Optimal multiple microgrids based forming of greenfield distribution network under uncertainty, IET Renewable Power Generation 11 (2017) 1059–1068.

[29] E. Vera, C. Canizares, M. Pirnia, J. Melo, T. Guedes, Two-stage stochastic optimization model for multi-microgrid planning, IEEE Transactions on Smart Grid (Accepted for publication on September 2022).

[30] IEEE Recommended Practice for the Planning and Design of the Microgrid, IEEE Std 2030.9-2019 (2019) 1–46.

[31] E. Vera, C. Canizares, M. Pirnia, Renewable energy integration in canadian remote community microgrids: The feasibility of hydrogen and gas generation, IEEE Electrification Magazine 8 (2020) 36–45.

[32] K. Høyland, S. W. Wallace, Generating scenario trees for multistage decision problems, Management Science 47 (2001) 295–307.
[33] S. Jin, S. M. Ryan, J.-P. Watson, D. L. Woodruff, Modeling and solving a large-scale generation expansion planning problem under uncertainty, Energy Systems (2011) 209–242.
[34] W. Bishop, T. H. Grubesic, Geographic Information, Maps, and GIS, Springer International Publishing, Cham, 2016, pp. 11–25.
[35] J. Bisschop, AIMMS Optimization Modeling: Integer Linear Programming Tricks, AIMMS B.V., 2021.
[36] I. Goodfellow, Y. Bengio, A. Courville, Deep Learning, MIT Press, 2016. http://www.deeplearningbook.org.
[37] A. Voulodimos, N. Doulamis, A. Doulamis, E. Protopapadakis, Deep learning for computer vision: A brief review, Hindawi, Computational Intelligence and Neuroscience (2018) 1–13.
[38] K. He, G. Gkioxari, P. Dollár, R. B. Girshick, Mask r-cnn, 2017 IEEE International Conference on Computer Vision (ICCV) (2017) 2980–2988.
[39] R. Alouta, K. Hess, Deep learning with arcgis pro tips and tricks, 2021. URL: http://https://www.esri.com/.
[40] ESRI, Automate building footprint extraction using deep learning, 2020. URL: http://https://www.esri.com/.
[41] PVsyst, Meteo databases, synthetic data generation (2022).
[42] J. A. Duffie, W. A. Beckman, Solar Engineering of Thermal Processes, 4 ed., John Wiley & Sons, Ltd, 2013.
[43] NASA, Prediction of worldwide resources, 2021. URL: power.larc.nasa.gov.